How far are global croplands from environmental sustainability ?

Supplementary information

Marcellin Guilbert[a], Silvia Ceaușu[b], Siyu Hou[c,d], Xu Zhao[d], Peiyu Cao[e], Franco Bilotto[e], Carlos Gonzalez Fischer[e], Mario Herrero[e], Carole Dalin[f,a]

[a] Laboratoire de Géologie, École normale supérieure, CNRS, PSL Université, IPSL, Paris, France

[b] Centre for Biodiversity and Environment Research, Department of Genetics, Evolution and Environment, University College London, London, UK

[c] Integrated Research on Energy, Environment and Society (IREES), Energy and Sustainability Research Institute Groningen (ESRIG), University of Groningen, Groningen, the Netherlands

[d] Institute of Blue and Green Development, Shandong University, Weihai, China

[e]Department of Global Development, College of Agriculture and Life Sciences, and Cornell Atkinson Center for Sustainability, Cornell University, Ithaca, NY, USA

[f] Institute for Sustainable Resources, University College London, London, UK

Corresponding author: Carole Dalin, carole.dalin@ucl.ac.uk

Extended methodology

Nitrogen

1) Crop-specific nitrogen application circa year 2020

Crop-specific nitrogen applications for 2020 are from Cao et al[1]. In that study, synthetic fertilizer application data were obtained for each crop category by combining synthetic nitrogen application data from FAO and crop-specific national-level synthetic application data from the International Fertilizer Association (IFA), along with subnational data for 40 countries. Cao et al. combined these national and sub-national scale datasets with MapSPAM

2020 to produce maps of synthetic nitrogen fertilizer application for 46 crop categories. Cao et al. then estimated gridded manure nitrogen (N) application rates in 2020, using livestock distributions from GLW v4.0 combined with animal-specific parameters from GLEAM and IPCC Tier 2 guidelines. N excretion was calculated by livestock type, region, and management system. Only managed manure considered available to croplands was retained, excluding burned or pasture-deposited manure. N Losses due to volatilization and leaching were accounted for following IPCC protocols. Final manure N rates were allocated evenly across cropland pixels and capped at 700 kg N ha^{-1} yr^{-1} when combined with synthetic fertilizer.

2) Nitrogen boundary

Nitrogen application limits in agricultural systems are from Schulte-Uebbing et al[2], in which three critical threshold concentrations were defined to avoid harmful impacts on terrestrial biodiversity, freshwater biodiversity, and drinking water quality. Nitrogen losses from agriculture leading to these critical concentrations were then estimated using the integrated assessment model IMAGE-GNM, which also accounts for nitrogen emissions from other sectors (e.g., industry, households). Finally, critical nitrogen applications on cropland were calculated by using nitrogen use efficiency.

To ensure consistency with nitrogen application from Cao et al[1], we downscaled critical nitrogen application from 30 arcminutes to 5 arcminutes (~10 km at the Equator). For each 30-arcminute parent cell, the total nitrogen boundary was uniformly allocated to all constituent 5-arcminute sub-cells identified as cultivated land according to the MapSPAM dataset, thereby restricting limits to agriculturally active areas while conserving the parent-cell total.

Because of temporal and categorical discrepancies between datasets, some 5-arcminute cells classified as cultivated in MapSPAM lacked an associated boundary value (for example due to recent cropland expansion or spatial mismatches). These cells were assigned the value of the nearest neighbouring valid grid cell using nearest-neighbour spatial interpolation to ensure complete spatial coverage.

To derive crop-specific constraints from the aggregated arable-land boundary, we implemented a sub-grid allocation scheme. Within each 5-arcminute cell, the downscaled nitrogen boundary was partitioned among crop types proportionally to their physical area shares in MapSPAM. This proportional allocation conserves the total nitrogen limit at the grid-cell level while generating crop-specific application ceilings consistent with the local land-use composition.

GHG

1) GHG emission 2020

GHG emissions from cropland for 2020 are from Cao et al[1], which estimated gridded global greenhouse gas (GHG) emissions in 2020 for 46 crop categories using the IPCC 2019 methodology[3]. From the emission sources of this dataset, we include direct and indirect N_2O emissions from synthetic fertilizer use, manure application, and crop residue incorporation; CH_4 emissions from rice cultivation; GHGs (N2O, CH4) from crop residues (burnt and not); and emissions from drained peatlands in Indonesia and Malaysia (CH4, N2O, CO2). Estimates account for variation by climate, crop type, water and nutrient management, and hydrological conditions. Emissions were expressed as CO_2 equivalents (CO_2e) based on 100-year Global Warming Potential (GWP) values from IPCC AR6.

2) GHG boundary

In this study, we draw upon the decarbonization pathways developed by Smith et al[4], which identify agricultural mitigation strategies consistent with limiting global warming to below 2 °C. Their analysis is implemented within the integrated assessment model IMAGE 3.0, which subdivides the world into 26 socio-economic regions (Fig.S1), and adopts the Shared Socioeconomic Pathway SSP2 ("middle-of-the-road"). Under SSP2, regional trajectories of population growth, GDP per capita, dietary preferences, and commodity prices are prescribed exogenously. These inputs feed the MAGNET module of IMAGE, a global computable general equilibrium model, which endogenously computes food demand and production volumes for each commodity in each region considering inter-regional food trade. Projected demand then drives IMAGE's land-use allocation algorithm, assigning cropland, pasture, forest, and bioenergy area on a 0.5° × 0.5° grid so as to satisfy regional production targets. Given the resulting land-use maps, the dynamic vegetation and crop-growth model LPJmL simulates greenhouse-gas emissions from eight crop functional types and five livestock products under region-specific management regimes. To ensure consistency with the 2 °C target, a global carbon price is imposed, forcing each region to remain within its allocated share of the cumulative agricultural emission budget derived from socio-economic factors from the SSP2 trajectory (GDP growth, population growth, etc…) . Regions may deploy any combination of thirty mitigation measures, whose costs and abatement efficacies vary from region to region, to meet their emission constraints in the most cost-effective manner. This modeling chain thus links socio-economic development, land-use change, and process-based emissions modeling to derive regionally differentiated, crop-specific decarbonization pathways for agriculture.

To assess the GHG sustainability of current cropland emissions, we derive region and crop specific emission boundaries based on 2050 targets from the Smith et al[4] analysis, thereby aligning our framework with mid-century climate objectives and ensuring policy relevance. While these targets account for projected increases in food demand, using them directly to benchmark current emissions could overstate sustainability by implicitly allowing higher emissions due to anticipated production growth. To correct for this, we calculate region-specific target carbon intensities (tCO_2e per ton of product) for the eight crop functional types

defined in IMAGE, consistent with each region's 2050 emission allowance. We then classify each MapSPAM crop category within these functional types (Table S1) and multiply the target carbon intensities by present-day production volumes.

This yields production-adjusted emission ceilings, which represent the emissions that would occur if current production levels were achieved under the crop- and region-specific emission intensities projected for a food system consistent with mid-century climate targets. Comparing current emissions to these ceilings quantifies the gap between present-day emission intensities and those implied by a specific future mitigation pathway limiting global warming to +2°C, conditional on assumptions regarding demand, technology, and cross-sector decarbonisation. Emissions from land-use change are excluded, except for peatland drainage in Indonesia and Malaysia. These spatially explicit, crop-specific GHG targets allow identification and prioritization of lower-intensity production systems across heterogeneous agricultural landscapes.

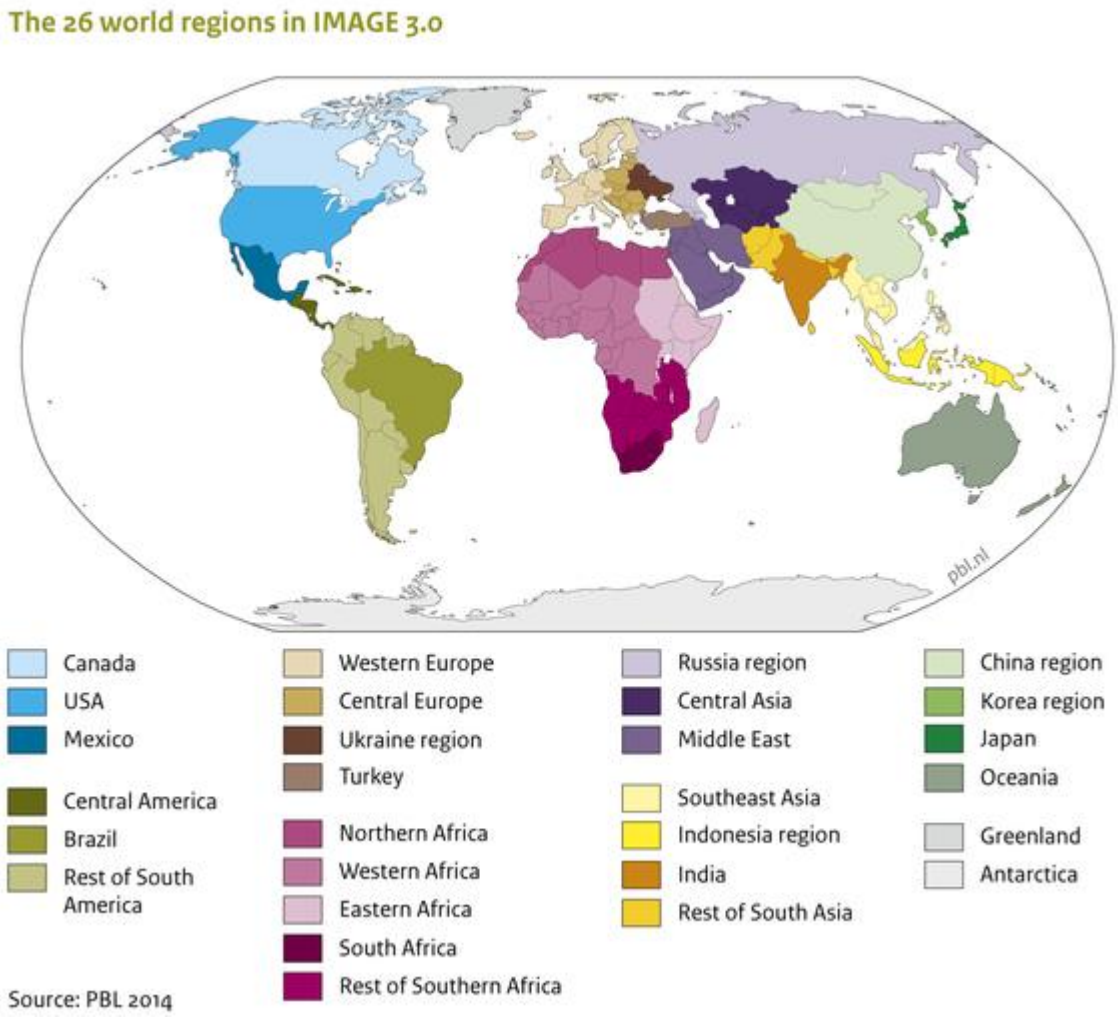

Fig.S1: The IMAGE framework region classification

Image category	MapSpam crops
Maize	Maize
Rice	Rice
Temperate cereals	Wheat, Barley, Other cereals
Tropical cereals	Millet, Sorghum
Roots and tubers	Potato, Sweet Potato, Yams, Cassava, Other Roots, Sugarbeet
Pulses	Bean, Chickpea, Cowpea, Pigeon pea, Lentil, Other pulses

Oil crops	Soybean, Groundnut, Coconut, Oilpalm, Sunflower, Rapeseed, Sesame seed, Other oil crops
Other crops	Sugarcane, Cotton, Other Fibre Crops, Arabic Coffee, Robust Coffee, Cocoa, Tea, Tobacco, Banana, Plantain, Citrus, Other Tropical Fruit, Temperate Fruit, Tomato, Onion, Other Vegetables, Rubber, Rest Of Crops

Table S1. Correspondence between IMAGE crop functional types and MapSpam crop categories

Human-Appropriation of Net Primary Production (HANPP)

Net Primary Production (NPP, tC) is the rate at which vegetation assimilates solar energy into biomass and constitutes the primary energy input that sustains terrestrial trophic networks. By fueling organismal growth, maintenance, and reproduction, NPP underpins critical ecosystem processes such as nutrient cycling and carbon sequestration. NPP serves as a quantifiable proxy for energy flow and so for ecosystem functionality[5].

1) HANPP estimates for 2020

NPP and Human Appropriation of Net Primary Production (HANPP) estimates for 2020 are from Matej et al[6] which developed LUIcube, a global dataset that tracks land-use change and intensity annually from 1992 to 2020 at a fine spatial resolution (30 arcseconds). It identifies 32 land-use classes, which can be aggregated into five main land-use types: cropland, grazing land, forestry, built-up land, and wilderness. Cropland is further divided into 22 crop categories (Table.S2).

To map land-use areas, Matej et al[6] refined existing methods by integrating the ESA Climate Change Initiative land cover product[7] with spatially explicit land-use data from the FAO[8], the Spatial Production Allocation Model (SPAM)[9], and various datasets capturing human presence and infrastructure.

To assess land-use intensity, the study applies the Human Appropriation of Net Primary Production (HANPP) framework[10]. In this framework, NPP_{act} corresponds to the current level of net primary production (in tC), while NPP_{pot} (tC) refers to NPP available in the hypothetical absence of human influence. In this context, $HANPP_{LUC}$ which is the biomass production lost due to land-use change is defined as:

$$HANPP_{LUC} = NPP_{pot} - NPP_{act} \quad \text{(Eq. 1)}$$

HANPP (in tC) which is the human appropriation of primary production is the sum of the flow of biomass inhibited by land-use change ($HANPP_{LUC}$) and of the harvested biomass ($HANPP_{harv}$):

$$HANPP = HANPP_{LUC} + HANPP_{harv} \quad \text{(Eq. 2)}$$

which also corresponds to NPP_{pot} minus the remaining NPP after harvest. Estimating these components involves combining modelled potential NPP (NPP in the absence of human use, or NPPpot) with actual biomass harvest data from FAO statistics for agriculture and forestry. This provides a consistent and spatially-explicit indicator of land-use intensity.

2) <u>HANPP boundary</u>

HANPP reduces the energy available to terrestrial trophic networks and, when it reaches certain levels, can thus impair essential ecosystem processes such as nutrient cycling and carbon storage, thereby compromising the functional integrity of the biosphere.

Richardson et al[11] define the planetary boundary for functional biosphere integrity as a level of HANPP equal to 10% of the pre-industrial potential NPP. As pre-industrial NPP estimates from Matej et al[6] are not available, we apply a correction factor to account for the ~20% global increase in NPP from the pre-industrial period to the present[11], resulting in a HANPP planetary boundary set at 8% of current potential NPP. We recognize, however, that this increase in NPP has not been spatially homogeneous, and that the absence of spatially explicit pre-industrial NPP data in LUIcube limits a more detailed evaluation.

To operationalize this boundary in our spatial analysis, we apply the 8% boundary uniformly at the grid-cell level as a local sustainability benchmark. While we acknowledge that local HANPP boundaries should ideally be grounded in local relationships between HANPP and ecosystem service provision, such refinement lies beyond the scope of this study. Nonetheless, as this limit is derived from a globally precautionary boundary, we consider it a conservative first-order approximation of sustainable biomass appropriation at finer scales.

To define a crop-specific HANPP limit, we distribute the local boundary proportionally to the HANPP of each of the 32 land-use classes. In a given grid-cell, the HANPP boundary for land-use type k is defined as :

$$HANPP_k^{boundary} = 0.08 * NPP_{pot} * \frac{NPP_k}{\sum_{i=1}^{32} NPP_i} \quad \text{(Eq. 3)}$$

By allocating more of the HANPP sustainable budget to systems exhibiting higher biomass extraction, namely intensive croplands, we acknowledge that these landscapes bear the brunt of human demand and thus warrant a larger allocation. At the same time, we recognize that anchoring allocations in current usage may reinforce existing production patterns, potentially slowing transitions.

Applying a uniform 8% global boundary without accounting for biome sensitivity may overestimate sustainable HANPP allowances in biodiversity-rich and ecologically sensitive regions such as tropical rainforests. Likewise, allocating the HANPP budget strictly according to current biomass extraction risks over-rewarding intensive monocultures, despite their low biodiversity and simplified trophic networks, and thus undermines ecological resilience. To address these limitations, we complement our NPP-based biosphere assessment with a second metric, species richness, which offers a structural measure of ecosystem integrity and explicitly captures both the biodiversity loss inherent to monocultures and the heightened vulnerability of tropical biomes.

HANPP category	**MapSpam2020**	**MapSpam2020 full name**
CL-BANP	BANA, PLNT	Banana, plantain
CL-BARL	BARL	Barley
CL-BEAN	BEAN	Bean
CL-CASS	CASS	Cassava
CL-COFF	COFF, RCOF	Arabic coffee, robust coffee
CL-COTT	COTT	Cotton
CL-GROU	GROU	Groundnut
CL-MAIZ	MAIZ	Maize
CL-MILL	PMIL, MILL	Pearled millet, small millet
CL-OFIB	OFIB	Other fiber crops
CL-OOIL	CNUT, OILP, SUNF, RAPE, SESA, OOIL	Coconut, oilpalm, sunflower, rapeseed, sesame, other oil crops
CL-OPUL	CHIC, COWP, PIGE, LENT, OPUL	Chickpea, cowpea, pigeon pea, lentil, other pulses
CL-POTA	POTA	Potato
CL-REST	OCER, ORTS, REST, COCO, TEAS, TOBA, RUBB	Other cereals, other roots, rest of crops, cocoa, tea, tobacco, rubber
CL-RICE	RICE	Rice

CL-SORG	SORG	Sorghum
CL-SOYB	SOYB	Soybean
CL-SUGB	SUGB	Sugarbeet
CL-SUGC	SUGC	Sugarcane
CL-SWPY	SWPO, YAMS	Sweet potato, yams
CL-VEFR	VEGE, TROF, TEMF, TOMA, ONIO, CITR	Other vegetables, other tropical fruit, temperate fruit, tomato, onion, citrus
CL-WHEA	WHEA	Wheat

Table S2: Correspondence between Matej et al[6] and MapSPAM2020 crop categories

Species richness

1) PREDICTS database

We used biodiversity data from the PREDICTS database (Projecting Responses of Ecological Diversity In Changing Terrestrial Systems)[12], which encompasses 2.9 million records, mostly sampled from 2000 to 2012, from 666 studies. Species included in the studies are vertebrates, invertebrates, fungi, slime, moulds and plants. These records document species-level metrics, including individual species abundance (83% of records), presence/absence (17% of records), or, less commonly, overall species richness (<1% of records) for assemblages sampled at specific sites along gradients of land use or land-use intensity.

The database is structured hierarchically: each study comprises data collected using consistent methods from one or more spatial blocks, which represent distinct spatial clusters. These blocks include data from multiple specific sites with geographical coordinates. At each site, records consist of species abundance, presence/absence, or richness data for individual taxa. The PREDICTS database is publicly accessible via the Natural History Museum's Data Portal (doi: http://dx.doi.org/10.5519/0073893). We calculated within-sample species richness (SR) as the total number of species recorded at each site.

To assess the influence of agricultural land on biodiversity relative to natural vegetation, we included sites classified under the land-use categories of primary vegetation, secondary vegetation, cropland, pasture, and plantation forest. Given the varying sensitivity of biodiversity to land use across regions[13], we further divided these sites into tropical and non-

tropical subsets based on latitude. Sites located between −23.44° and 23.44° latitude (the Tropics of Capricorn and Cancer) were classified as tropical, while those outside this range were designated as non-tropical. This classification resulted in two subsets: the tropical subset, comprising species richness estimates from 9505 sites across 306 studies, and the non-tropical subset, comprising species richness estimates from 11684 sites across 339 studies.

2) Food systems variables

To estimate the impact of agricultural cultivation on biodiversity, we focused on the influence of three variables across tropical and non-tropical biomes:

- Land-use
- Fraction of natural habitat
- Fertilizer application.

Our objective was to project these impacts globally, at high spatial resolution in 2020. Accordingly, we selected datasets that provide appropriate spatial and temporal coverage for each variable.

Land-use at each site was classified using habitat descriptions from the PREDICTS database[12]. PREDICTS categories include:

- Primary vegetation (PV): natural habitat with no known historical disturbance;
- Secondary vegetation (SV): recovering habitat previously disturbed by human activity or natural events;
- Plantation forest (PF): areas used for cultivation of woody crops (e.g. oil palm, coffee, timber);
- Cropland (Crop): land used for herbaceous crops (including livestock fodder);
- Pasture (Past): land regularly or permanently used for livestock grazing.

To project land-use categories globally, we used the LUH2 dataset[14], which provides global land-use maps from 850 to 2100 at ~25 km spatial resolution. We regrouped LUH2 land-use categories to match the PREDICTS classification (see Table S3). To ensure consistency with

other datasets, LUH2 data were downscaled to 5 arcminutes (~9 km at the Equator) using nearest-neighbor interpolation (i.e. assigning the value of the closest pixel).

The fraction of natural habitat was also derived from LUH2. We computed it as the sum of land-cover fractions for primary and secondary vegetation in each grid cell. PREDICTS site coordinates were then overlaid on this map to extract the local natural habitat fraction, which was used in subsequent statistical models.

For fertilizer application we used data from EarthStat[15] and Cao et al[1], which provide fertilizer application maps for different crops for 2000 and 2020 respectively, that we aggregated to obtain total fertilizer application estimates.

PREDICTS	LUH2
Primary Vegetation (PV)	primf - Primary forest
	primn - Primary non-forest
Secondary Vegetation (SV)	secdf - Secondary forest
	secdn - Secondary non-forest
Cropland (Crop)	c3ann - C3 annual crops
	c4ann - C4 annual crops
	c3nfx - C3 nitrogen-fixing crops
Pasture (Past)	pastr - Managed pasture
	range - Rangeland
Plantation Forest (PF)	c3per - C3 perennial crops
	c4per - C4 perennial crops

Table S3. Correspondence between LUH2 and PREDICTS land-use categories

3) Statistical model and analysis

Species richness was modeled using generalized linear mixed-effects models (GLMMs) with Poisson-distributed errors. Random effects were included to account for potential sources of variation: study identity accounted for differences in sampling methods, taxonomic groups, and geographical regions; spatial block within study accounted for the spatial arrangement of sampling sites[16]; and site identity, nested within spatial block and study, was included to account for overdispersion[16,17].

All two-way interactions were included in the models. Total fertilizer application estimates were ln-transformed (with one added to handle zero values) to reduce skewness and all continuous variables were standardized to have a mean of zero and a standard deviation of one. The optimal fixed-effects structure was identified through backward stepwise model selection, using likelihood-ratio (χ^2) tests to assess the inclusion of each variable. The model was calibrated using data for the year 2000 to align with the sampling period of the PREDICTS database.

To evaluate the robustness of the results, we compared the final Poisson GLMM to two alternative models. A GLMM with a negative binomial distribution produced nearly identical results. A Bayesian model yielded slightly different coefficient estimates, but the 95% credible intervals overlapped with the Poisson model coefficients, supporting the robustness of our conclusions. (see Table.S4)

All statistical analyses were performed in R v.4.3.3 (R Core Team, 2024). The models were implemented in R using the glmmTMB package v.1.1.10[18]. Diagnostic checks were conducted to verify model assumptions and assess spatial autocorrelation in the residuals (Fig.S2).

Predictions of species richness for 2020 were generated using the calibrated model, with land use, natural habitat fraction, and fertilizer application corresponding to 2020 conditions as explanatory variables, by sampling 1000 estimates from the variance–covariance matrix.

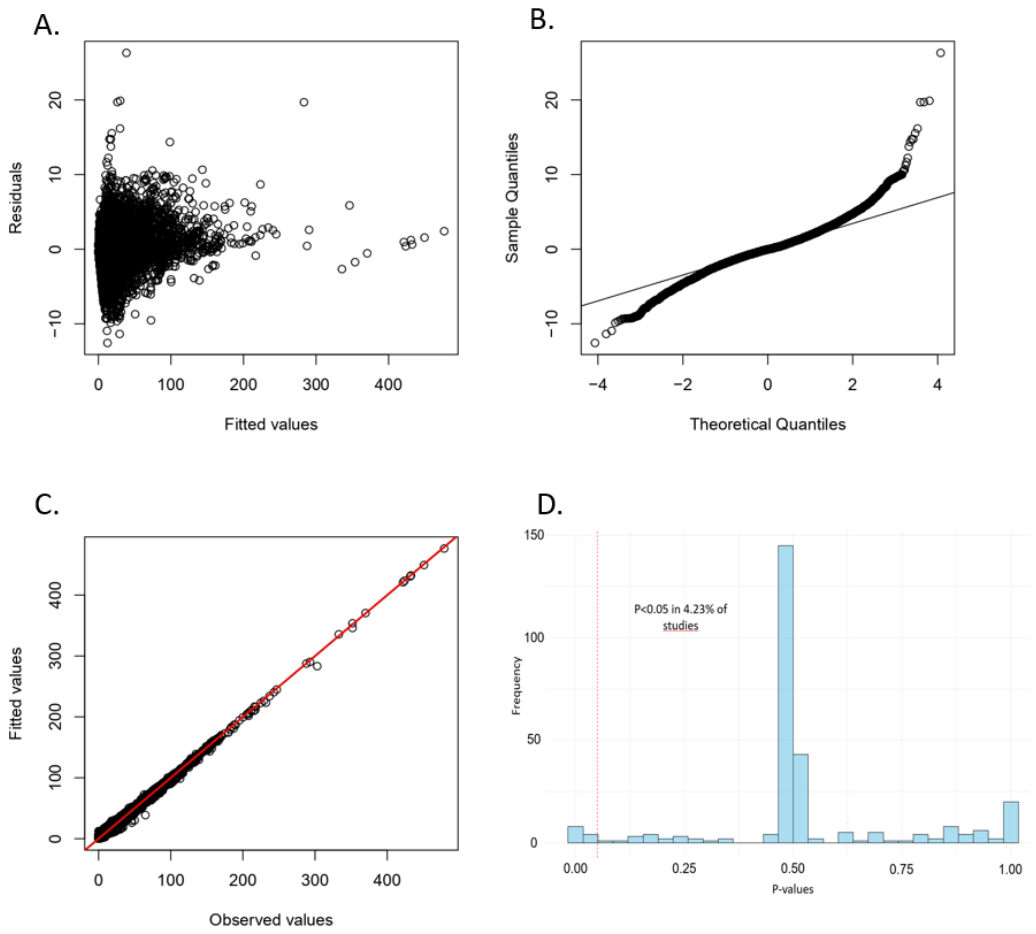

Fig S2. Species richness model checks. A. Fitted vs. residuals plot to check for constant variance across the range of fitted values. B. Q-Q plot to check the normality of the residuals. C. Plot of observed vs predicted values (predicted values incorporate both fixed and random effects). D. Histograms of P values from sets of Moran's tests for spatial autocorrelation in the residuals of the best models for individual studies. The red line represents P = 0.05. By chance, we expect to detect significant spatial autocorrelation in the residuals associated with 5% of studies.

Terms	Poisson estimate	Negative binomial estimate	Bayesian estimate	Bayesian credible interval	Significance
Intercept	2.68	2.72	2.68	[2,55;2,82]	***
PLU-SV	-0.11	-0.11	-0.11	[-0,14; -0,08]	***
PLU-Pasture	-0.41	-0.40	-0.41	[-0,45; -0,36]	***

PLU-Cropland	-0.31	-0.30	-0.32	[-0,36; -0,27]	***
PLU-PF	-0.28	-0.28	-0.29	[-0,32; -0,25]	***
Biome-nonTropical	-0.08	-0.09	-0.09	[-0,26;0,09]	
percNHRS	8.04	7.59	7.81	[4,12; 11,52]	***
fert_logRS	5.57	5.58	3.13	[-0,61;6,64]	**
PLU-SV:Biome-nonTropical	-0.06	-0.05	-0.05	[-0,1;-0,01]	*
PLU-Pasture:Biome-nonTropical	0.23	0.23	0.25	[0,19;0,3]	***
PLU-Cropland:BiomeNonTropical	0.01	0.01	0.02	[-0,04;0,09]	
PLU-PF:BiomeNonTropical	0.09	0.08	0.09	[0,02;0,16]	*
PLU-SV:percNHRS	-1.17	-1.07	-0.34	[-3,03;2,38]	
PLU-Pasture:percNHRS	-12.52	-12.07	-10.72	[-14,28;-7,19]	***
PLU-Cropland:percNHRS	2.00	2.20	2.41	[-1,98;6,66]	
PLU-PF:percNHRS	-8.16	-8.22	-6.74	[-10,57;-2,82]	***
Biome-nonTropical:percNHRS	12.00	11.55	10.26	[5,57;15,08]	***
PLU-SV:fert_logRS	-8.11	-7.81	-6.67	[-9,6;-3,7]	***
PLU-Pasture:fert_logRS	-10.40	-10.26	-8.80	[-12,26;-5,25]	***
PLU-Cropland:fert_logRS	1.65	1.73	2.39	[-2,51;7,35]	
PLU-PF:fert_logRS	-11.08	-10.90	-8.58	[-12,43;-4,81]	***
Biome-nonTropical:fert_logRS	-6.73	-6.94	-5.03	[-9,19;-1,1]	**

Table S4. Species richness model robustness checks. Coefficients and credible intervals of the Poisson, Negative binomial and Bayesian models. *** corresponds to p-value < 0.001; ** corresponds to 0.001 < p-value ≤ 0.01; * corresponds to 0.01 < p-value ≤ 0.05. PLU stands for Predominant Land-use, perNHRS is the standardized fraction of natural habitat, fert_logRS is the log-transformed and standardized fertilizer application.

4) Species richness sustainability

a) Crop-specific species richness loss

While species richness alone cannot capture the full complexity of biodiversity critical to ecosystem functioning, it remains a key indicator. It has been identified as a major driver affecting essential ecosystem processes such as primary production and decomposition, which are critical to the global carbon cycle and the provision of numerous ecosystem services. Species richness captures the biotic consequences of environmental pressures (how biodiversity responds to human land use) and is used in this study as a complementary metric to HANPP, explicitly to address limitations of the HANPP framework. For instance conversion to intensively managed cropland may not lead to significant NPP change, and thus in HANPP, but likely leads to significant species loss. Hence in such cases, species richness captures impacts on the biosphere that HANPP alone may overlook, helping to provide a more complete picture of ecological change.

In a given grid cell:

$$SR_{actual} = \frac{\alpha_{PV}SR_{PV}+\alpha_{SV}SR_{SV}+\alpha_{Crop}SR_{Crop}+\alpha_{Past}SR_{Past}+\alpha_{PF}SR_{PF}}{\alpha_{Tot}} \ (Eq.4)$$

Where α_i is the fraction covered by land-use type i and SR_i the species richness in land-use type *i* estimated from our statistical modelling.

Relative changes in species richness are determined by comparing current richness with a baseline approximated as the richness that would occur if all land were primary vegetation and without fertilizer application:

$$\Delta SR = \frac{SR_{actual}-SR_{baseline}}{SR_{baseline}} \ (Eq.5)$$

$$\Delta SR = \frac{\alpha_{SV}(SR_{SV}-SR_{PV}^{baseline})+\alpha_{Crop}(SR_{Crop}-SR_{PV}^{baseline})+\alpha_{Past}(SR_{Past}-SR_{PV}^{baseline})+\alpha_{PF}(SR_{PF}-SR_{PV}^{baseline})+\alpha_{PF}(SR_{PV}-SR_{PV}^{baseline})}{\alpha_{Tot}SR_{PV}^{baseline}} \ (Eq.6)$$

Which can be written as:

$$\Delta SR = \Delta SR_{SV} + \Delta SR_{Crop} + \Delta SR_{Past} + \Delta SR_{PF} + \Delta SR_{PV} \ (Eq.7)$$

Where:

$$\Delta SR_i = \frac{\alpha_i(SR_i-SR_{PV}^{baseline})}{\alpha_{Tot}SR_{PV}^{baseline}} \ (Eq.8)$$

ΔSR_i represents the contribution of a given land-use type to the relative change in species richness in a given grid-cell (Fig.S3). To derive crop-specific metrics, the species richness loss attributed to Cropland and Plantation Forest is then distributed among individual crops depending on their classification (Table.S5) and in proportion to their cultivated area, as reported by MapSPAM 2020

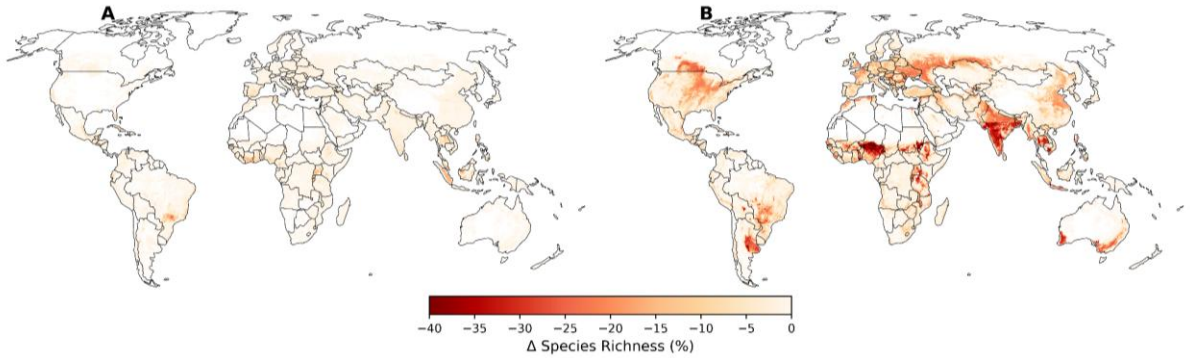

Fig S3. Species richness loss to plantation forest (a) and cropland (b).

b) Species richness boundary

Hooper et al[19] suggest that a 20% reduction in species richness marks a reference boundary beyond which biodiversity loss may impair ecosystem functioning. Accordingly, we adopt a 20% decline in species richness as the sustainability threshold at the grid-cell level. To define a biodiversity limit in a crop-specific manner, this boundary must be partitioned among competing land uses and crops within each grid cell.

First, the boundary was allocated among land-use types within each grid cell in proportion to the species richness loss attributable to each land use (see Eq. 8). In a given grid-cell, the boundary for species richness loss attributed to land-use k is calculated as:

$$\Delta SR_k^{boundary} = 20\% * \frac{\Delta SR_k}{\sum_i \Delta SR_i} \text{ (Eq. 9)}$$

where ΔSR_k is the species richness loss associated to land-use type k and $\sum_i \Delta SR_i$ is the total species richness loss within the cell.

Next, crops from MapSPAM are classified as either Cropland or Plantation Forest, distinguishing between perennial and annual crops (Table S5). The species richness loss boundary allocated to Cropland or Plantation Forest in the previous step is then distributed among individual crops proportionally to their cultivated area in each grid-cell, as reported by MapSPAM 2020. For a given crop c classified as Cropland with a cultivated area A_c, the species richness loss boundary is:

$$\Delta SR_c^{boundary} = \Delta SR_{cropland}^{boundary} * \frac{A_c}{\sum_i A_i} \text{ (Eq. 10)}$$

where the denominator $\sum_i A_i$ represents the total cultivated area of all crops classified as cropland within the grid cell (Table.S5). The same allocation logic is applied to crops classified as plantation forests, ensuring their individual boundaries are proportional to their respective shares of total plantation area.

Cropland	Plantation Forest
Wheat	Coconut
Rice	Oilpalm
Maize	Sugar cane
Barley	Arabica coffee
Small millet	Robusta coffee
Pearled millet	Cocoa
Sorghum	Tea
Other cereals	Banana
Potatos	Plantain
Sweet potato	Citrus
Yams	Other tropical fruits
Cassava	Temperate fruits
Other roots	Rubber
Bean	
Chickpea	
Cowpea	
Lentils	
Other pulses	
Soybean	
Groundnut	
Sunflower	
Rapeseed	
Sesame	
Other Oil crops	
Sugarbeet	
Cotton	
Other Fibers	
Tomato	
Onion	
Other vegetables	
Rest of crops	
Tobacco	

Table S5. Correspondence between MapSpam crops and LUH2 land-use categories

Freshwater

To evaluate the sustainability of Cropland water use, we focus on freshwater withdrawal for irrigation, and compare it with the Regional Freshwater Boundaries (RFBs)[20]. These boundaries are based on Environmental Flow Requirements (EFRs) which represent the portion of river flow that should remain untouched to preserve ecosystem integrity[21], and freshwater withdrawal data from both agricultural and non-agricultural sectors. The evaluation of both water withdrawal and Regional Freshwater Boundaries is based on Hou et al[20].

1) Water Withdrawal in 2020

In this study, we estimated water withdrawal using both the WaterGAP3[22,23] and WaterGAP2[24] datasets, each distinguishing five sectors: irrigation, livestock (including drinking and cleaning), manufacturing, electricity (cooling in thermoelectric power plants), and domestic use (households and services). While WaterGAP2 provides the most recent withdrawal estimates (up to 2019), its spatial resolution (30 arcminutes) is coarser than that of WaterGAP3 (5 arcminutes). To align with the higher-resolution datasets used elsewhere in this study, we applied a downscaling approach, using the 5-arcminute WaterGAP3 data available up to 2015 to spatially disaggregate the 2019 WaterGAP2 data. This method preserves fine-scale spatial heterogeneity while incorporating the most up-to-date withdrawal estimates.

We downscaled the 2019 water withdrawal data for the five sectors from a spatial resolution of 30 arcminutes to 5 arcminutes. Each coarse 30-arcminute grid cell was subdivided into 36 finer 5-arcminute grid cells. When the 2019 withdrawal value was available for a coarse grid cell and the corresponding 36 finer grid cells in the 2015 data contained nonzero values, we allocated the 2019 withdrawal proportionally according to the 2015 spatial distribution across these finer cells. In cases where the 2019 coarse grid cell had a value but all corresponding 2015 finer grid cells were zero or missing, the 2019 withdrawal value was distributed evenly across all 36 finer cells.

The 2019 downscaled WaterGAP2 dataset is used as a proxy for water withdrawal in 2020, assuming minimal year-to-year changes[22].

2) Water sustainability boundary

Water sustainability was defined using RFBs, which were estimated by Hou et al.[20] using a bottom-up approach by allocating proportions of mean monthly flows (MMFs) to Environmental Flow Requirements (EFRs) across distinct flow seasons at a 5 arc-minute grid resolution. EFRs are estimated as the ensemble mean of 75 models, derived from the MMFs of 15 global hydrological models following ISIMIP2a protocols over 1970–2010 by applying five hydrological methods (Tessmann, VMF, Tennant, Q90_Q50, Smakhtin)[25], which segment the year into high, intermediate, and low flow periods. This approach using a multi-model and

multi-method ensemble average, helps reduce uncertainties in the assessment of RFBs[20]. Monthly RFBs were aggregated annually to match water withdrawal data, so that in a given grid-cell :

$$RFB = \sum_{i=1}^{12}(MMF_i - EFR_i) \quad ; \; where\ i\ is\ a\ month\ (Eq\ .11)$$

3) Crop-specific irrigation water withdrawal and boundaries

When water withdrawal exceeds the RFBs, freshwater resources are depleted. RFB exceedance is the difference between water withdrawal and the RFBs. It represents the extent of freshwater overuse when positive, and is set to zero when negative as it indicates sustainable water use.

To attribute sectoral responsibility for unsustainable water use, Hou et al[20] allocate the RFBs exceedance proportionally to each sector's water withdrawal. In our approach, we allocate the RFBs themselves proportionally to each sector's water withdrawal, which results in mathematically identical RFBs exceedances but allows the definition of sector-specific sustainability boundaries. For croplands, the RFB is assigned according to the irrigation contribution within each grid cell:

$$RFB_{irr} = RFB * \frac{WW_{irr}}{\sum_k WW_k} \; ; \; where\ k\ is\ a\ sector\ (Eq\ .12)$$

To go further and achieve a crop-specific sustainability assessment, we further allocated cropland RFB (RFB_{irr}) and water withdrawal among crop categories using their blue water footprint. We used data from Mialyk et al[26], which provides production and blue water intensity (m^3/ton) for 162 non-fodder crops in 2019 (Supplementary Data 1 for correspondence with MapSPAM crop categories). By calculating a production-weighted average, we derived blue water intensity for all MapSPAM categories, then multiplied these values by MapSPAM production data to estimate the blue water footprint (m^3) for each of the 46 MapSPAM crop categories. Both the cropland RFB and water withdrawal were then distributed among these crop categories proportionally to their blue water footprint within each grid cell, allowing for a detailed, crop-specific assessment of freshwater sustainability limits and use.

Extended results

		Fraction of production cultivated in cropland within sustainability limits (in %)					
Region	**Crop**	**GHG**	**Nitrogen**	**Species richness**	**HANPP**	**Freshwater**	***Irrigated Production***
Asia-Oceania	Rice	28.0	10.6	10.7	3.1	68.5	*82.5*
Asia-Oceania	Oil crops	61.7	67.6	9.7	85.1	98.1	*2.7*
Asia-Oceania	Maize	87.2	6.8	12.4	4.5	61.1	*44.0*
Asia-Oceania	Wheat	91.3	5.7	3.5	17.3	37.3	*75.6*
Asia-Oceania	Sugarcane	65.6	10.3	6.4	18.6	53.7	*76.3*
Africa-Middle East	Maize	64.7	44.5	7.6	17.5	88.7	*15.8*
Africa-Middle East	Cassava	48.8	80.7	14.8	14.1	99.9	*0.0*
Africa-Middle East	Wheat	89.5	15.3	21.8	30.4	49.3	*57.8*
Africa-Middle East	Oil crops	83.2	72.5	7.6	18.2	93.0	*7.6*
Africa-Middle East	Rice	47.8	51.0	9.3	23.6	78.3	*53.3*
Europe-Central-Asia	Wheat	89.3	20.4	14.2	1.2	93.9	*6.6*
Europe-Central-Asia	Maize	97.2	10.0	9.9	1.0	88.8	*20.8*
Europe-Central-Asia	Barley	85.3	17.5	16.5	0.8	95.3	*6.0*

Europe-Central-Asia	Oil crops	87.7	27.2	10.6	0.3	95.0	*6.1*
Europe-Central-Asia	Sugarbeet	99.1	10.6	11.7	0.2	92.8	*18.8*
North America	Maize	83.8	8.2	4.3	0.6	88.1	*18.6*
North America	Soybean	98.4	76.8	5.4	0.2	95.1	*10.2*
North America	Wheat	90.8	7.9	5.3	0.8	88.5	*13.4*
North America	Sugarcane	67.1	65.1	10.2	1.9	85.6	*54.3*
North America	Oil crops	66.4	19.0	8.8	23.0	96.5	*4.7*
South America	Sugarcane	33.3	57.8	3.4	1.9	97.3	*15.0*
South America	Soybean	89.8	83.4	11.8	1.7	99.8	*1.8*
South America	Maize	80.9	35.5	12.1	4.4	98.0	*8.6*
South America	Wheat	60.2	22.1	8.4	0.6	98.7	*2.9*
South America	Rice	31.8	25.3	15.0	10.3	90.1	*72.5*

Table.S6: Sustainability of major crops over 5 world regions. Fraction of production occurring over sustainably managed cropland (sustainability indicator below or equal to 1) for 5 environmental dimensions and fraction of irrigated production for the five most produced crops of each world region.

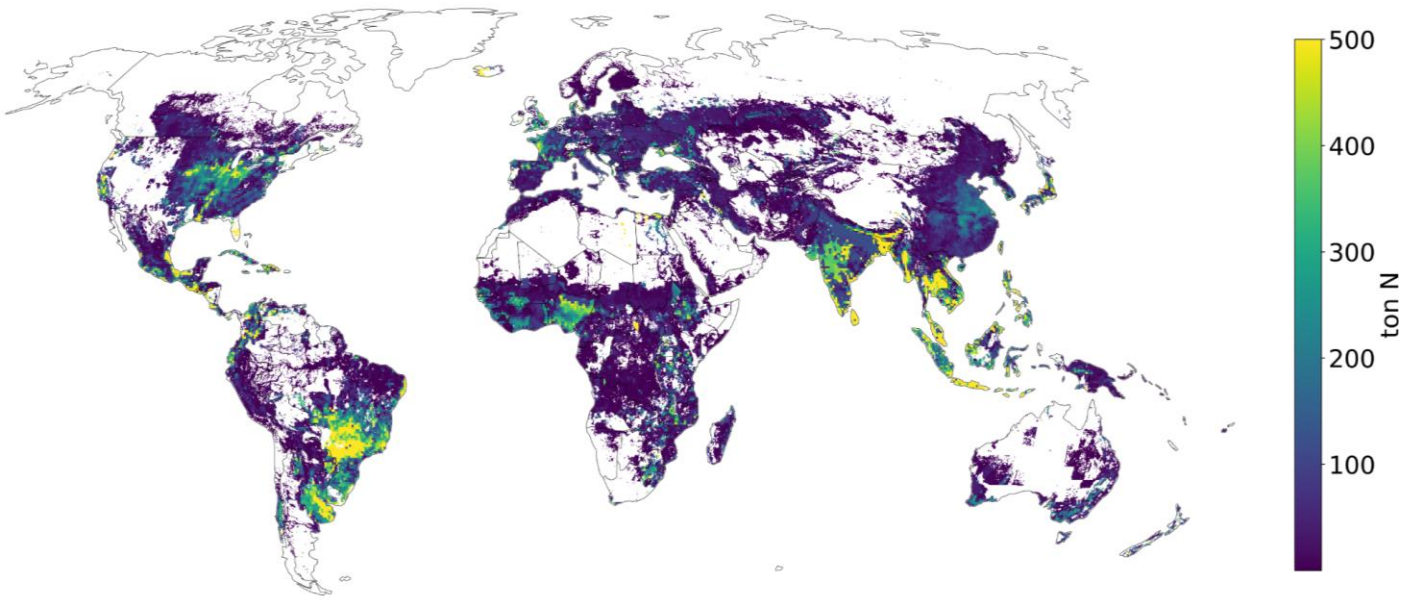

Fig.S4: Nitrogen application limit (in ton N) for global cropland

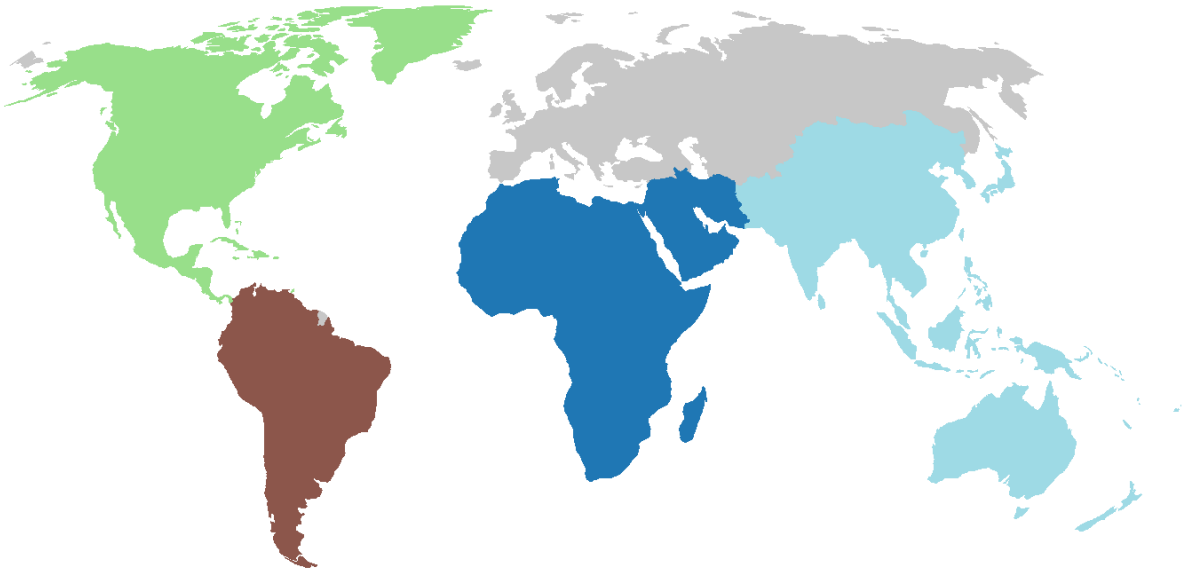

Fig.S5. Map representing the regions used in the regional-scale analysis. Regions are North America (green), South America (brown), Africa-Middle East (blue), Europe-Central Asia (grey) and Asia-Oceania (turquoise)

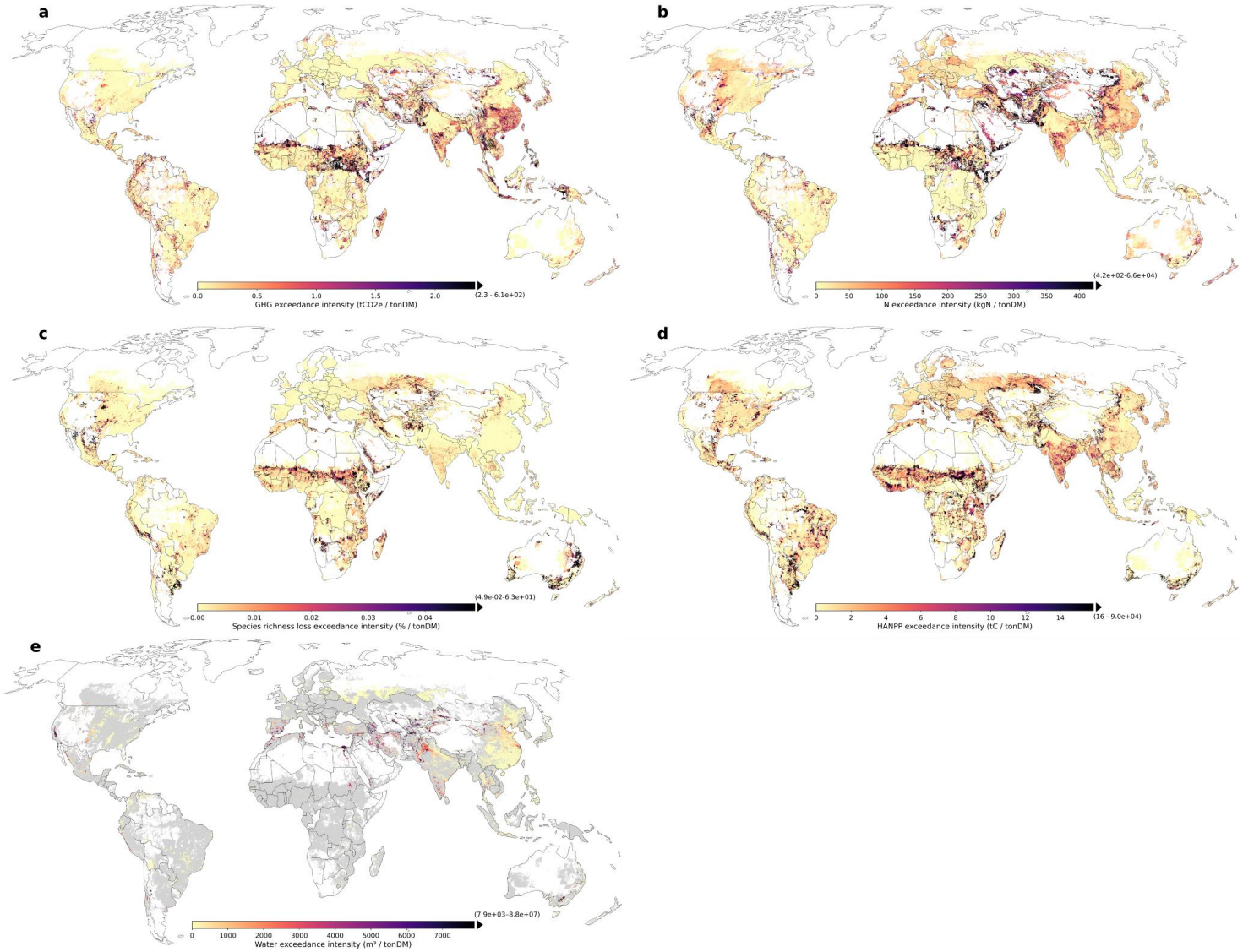

Fig.S6. Global maps of cropland environmental exceedance intensity. Ratio between environmental exceedance and production of crops in dry matter tonnes (tonDM) for GHG emissions (a), nitrogen application (b), species richness loss (c), HANPP (d) and freshwater use (e).

References

1. Cao, P. *et al.* Mapping greenhouse gas emissions from global cropland circa 2020. Preprint at https://doi.org/10.21203/rs.3.rs-6622054/v1 (2025).

2. Schulte-Uebbing, L. F., Beusen, A. H. W., Bouwman, A. F. & de Vries, W. From planetary to regional boundaries for agricultural nitrogen pollution. *Nature* **610**, 507–512 (2022).

3. Chapter 5 : Food Security — Special Report on Climate Change and Land. https://www.ipcc.ch/srccl/chapter/chapter-5/.

4. Smith, P. *et al. Science-Based GHG Emissions Targets for Agriculture and Forestry Commodities*. https://abdn.elsevierpure.com/files/141980461/38830_UoA_IBES_Report_v3.pdf (2016).

5. Pereira, H. M. *et al.* Essential Biodiversity Variables. *Science* **339**, 277–278 (2013).

6. Matej, S. *et al.* A global land-use data cube 1992–2020 based on the Human Appropriation of Net Primary Production. *Sci. Data* **12**, 511 (2025).

7. Copernicus Climate Change Service. Land cover classification gridded maps from 1992 to present derived from satellite observations. ECMWF https://doi.org/10.24381/CDS.006F2C9A (2019).

8. FAOSTAT. https://www.fao.org/faostat/en/#home.

9. Institute, I. F. P. R. Global Spatially-Disaggregated Crop Production Statistics Data for 2020 Version 1.0. https://doi.org/10.7910/dvn/swpent (2024) doi:10.7910/dvn/swpent.

10. Haberl, H., Erb, K.-H. & Krausmann, F. Human Appropriation of Net Primary Production: Patterns, Trends, and Planetary Boundaries. *Annu. Rev. Environ. Resour.* **39**, 363–391 (2014).

11. Richardson, K. *et al.* Earth beyond six of nine planetary boundaries. *Sci. Adv.* **9**, eadh2458 (2023).

12. Hudson, L. N. *et al.* The PREDICTS database: a global database of how local terrestrial biodiversity responds to human impacts. *Ecol. Evol.* **4**, 4701–4735 (2014).

13. Newbold, T., Oppenheimer, P., Etard, A. & Williams, J. J. Tropical and Mediterranean biodiversity is disproportionately sensitive to land-use and climate change. *Nat. Ecol. Evol.* **4**, 1630–1638 (2020).

14. Hurtt, G. C. *et al.* Harmonization of global land use change and management for the period 850–2100 (LUH2) for CMIP6. *Geosci. Model Dev.* **13**, 5425–5464 (2020).

15. Nutrient Application for Major Crops. *EarthStat* http://www.earthstat.org/nutrient-application-major-crops/.

16. Newbold, T. *et al.* Global effects of land use on local terrestrial biodiversity. *Nature* **520**, 45–50 (2015).

17. Rigby, R. A., Stasinopoulos, D. M. & Akantziliotou, C. A framework for modelling overdispersed count data, including the Poisson-shifted generalized inverse Gaussian distribution. *Comput. Stat. Data Anal.* **53**, 381–393 (2008).

18. Brooks, M. E. *et al.* glmmTMB Balances Speed and Flexibility Among Packages for Zero-inflated Generalized Linear Mixed Modeling. *R J.* **9**, 378–400 (2017).

19. Hooper, D. U. *et al.* A global synthesis reveals biodiversity loss as a major driver of ecosystem change. *Nature* **486**, 105–108 (2012).

20. Hou, S. *et al.* Tracking grid-level freshwater boundary exceedance along global supply chains from consumption to impact. *Nat. Water* 1–10 (2025) doi:10.1038/s44221-025-00420-z.

21. Steffen, W. *et al.* Planetary boundaries: Guiding human development on a changing planet. *Science* **347**, 1259855 (2015).

22. Flörke, M. *et al.* Domestic and industrial water uses of the past 60 years as a mirror of socio-economic development: A global simulation study. *Glob. Environ. Change* **23**, 144–156 (2013).

23. Flörke, M., Schneider, C. & McDonald, R. I. Water competition between cities and agriculture driven by climate change and urban growth. *Nat. Sustain.* **1**, 51–58 (2018).

24. Müller Schmied, H. *et al.* The global water resources and use model WaterGAP v2.2e: description and evaluation of modifications and new features. Preprint at https://doi.org/10.5194/gmd-2023-213 (2023).

25. Pastor, A. V., Ludwig, F., Biemans, H., Hoff, H. & Kabat, P. Accounting for environmental flow requirements in global water assessments. *Hydrol. Earth Syst. Sci.* **18**, 5041–5059 (2014).

26. Mialyk, O. *et al.* Water footprints and crop water use of 175 individual crops for 1990–2019 simulated with a global crop model. *Sci. Data* **11**, 206 (2024).